Distribution of [1,2-3H]cholesterol in mouse brain after injection in the suckling period

DISTRIBUTION OF [1,2-^{3}H]CHOLESTEROL IN MOUSE BRAIN AFTER INJECTION IN THE SUCKLING PERIOD

E. TESSA HEDLEY WHYTE

From the Department of Neurology-Neuropathology, Harvard Medical School, and the Department of Pathology (Neuropathology), The Children's Hospital Medical Center, Boston, Massachusetts 02115

ABSTRACT

Glutaraldehyde-carbohydrazide polymer (GACH) was used to embed olfactory tracts, trapezoid body, and sciatic nerves of 9-, 10-, and 49-day old mice 2 h, 24 h, and 6 wk (respectively) after the intraperitoneal administration of [1,2-^{3}H]cholesterol. Greater than 94% of radioactive cholesterol was retained in the GACH-infiltrated brain 24 h or more after injection. The fine structural preservation of both central and peripheral nervous tissues was excellent. Quantitative analysis of electron microscope autoradiographs demonstrated that [1,2-^{3}H]cholesterol is limited to blood vessel walls and lumen within the central nervous system at 2 h after administration. Myelin is the most highly labeled neural structure at both 24 h and 6 wk postinjection, but neurons and neuropil also contain the labeled cholesterol. The thickest myelin sheaths in the adult mice appear to be uniformly labeled throughout their width. No relationship of the retained [1,2-^{3}H]cholesterol to the node of Ranvier was found in the adult sciatic nerve.

[1,2-^{3}H]Cholesterol administered to suckling mice can be found within the peripheral nerve at maturity (14, 15, 28). Although the myelin sheaths were the most highly labeled structures within the mature nerve, labeled cholesterol was also present external to the myelin sheath and possibly within the axon as well (15). Rawlins et al. (28) found [1,2-^{3}H]cholesterol in both the regenerated and normal myelin sheaths of the sciatic nerve after Wallerian degeneration and regeneration induced in mice given the [1,2-^{3}H]cholesterol during myelination.

Biochemical studies of cholesterol turnover and incorporation in nervous tissues have concentrated on the brain (1, 3–7, 10, 20, 25, 27, 36, 38–40). Recently, evidence has been presented indicating the existence of a pool of cholesterol, which is being continually exchanged, within the central nervous system (1, 7, 10, 20, 25, 36, 39, 40) in addition to a stable metabolic pool (1, 3–7, 10, 20, 25, 36, 39, 40).

Biosynthetic cholesterol in the adult rat and cholesterol retained from infancy to adulthood in mouse brain were found mainly in white matter in frozen sections of Formalin-fixed (43) and unfixed brains (10, 37). The cellular structures with which the cholesterol was associated could not be resolved in these experiments. Attempts by us (unpublished) to explore the distribution of cholesterol in epoxy-embedded mouse brain were hampered by the small proportion of the administered dose which entered the brain and the 60–90% extraction which occurred during dehydration and embedding in Epon-Araldite (16).

The distribution of [1,2-^{3}H]cholesterol in peripheral nerve and lung was examined in autoradiographs of epoxy-embedded tissue (2, 15, 26, 28). Cholesterol is soluble in the epoxy resins as well as

in the organic solvents utilized for dehydration and infiltration of tissues before epoxy embedment (2, 9, 14, 16, 42), allowing for possible redistribution of the radioactive cholesterol during tissue processing. However, we found similar distributions of [1,2-^{3}H]cholesterol in frozen sections, epoxy-embedded partially dehydrated tissues (18), and epoxy-embedded regularly dehydrated tissues (2, 15). Despite these observations, Gautheron and Chevallier have commented that all studies of cholesterol utilizing an epoxy embedment are questionable (9).

Several methods are now available using glutaraldehyde polymers as embedding media so that all organic solvents are avoided (13, 24). Preliminary experiments indicated that glutaraldehyde-carbohydrazide (GACH) (13) gave a polymer which was easier to section than the glutaraldehyde-urea polymer (24), although the latter is easier to prepare. We decided, therefore, to investigate the cellular distribution of [1,2-^{3}H]cholesterol in mouse brain after administration to the suckling mouse. Evidence that GACH is a suitable medium for autoradiographic localization of cholesterol in addition to phospholipid (13) is also presented.

MATERIALS AND METHODS

Five Swiss albino mice were injected intraperitoneally with 0.2 ml of [1,2-^{3}H]cholesterol (approximately 140 μCi/g body weight) at 8, 10, and 12 days of age for a total dose of 570 μCi and were sacrificed 6 wk later. Six more mice from two litters were injected intraperitoneally (0.2 ml) at 9 days of age (260 μCi, approximately 70 μCi/g [litter 1] or 590 μCi, approximately 140 μCi/g [litter 2] per mouse); and three were sacrificed at 2 h and three at 24 h postinjection. Littermates injected with 0.2 ml of 4% dimethyl formamide in 5% dextrose and water were sacrificed with all litters.

[1,2-^{3}H]Cholesterol (specific activity 52.6 Ci/mmol, New England Nuclear, Boston, Mass.), obtained in benzene solution, was evaporated to dryness under a stream of dry air at 60°C. The cholesterol was dissolved in dimethyl formamide and subsequently diluted to a final concentration of 4% dimethyl formamide in 5% dextrose and water (2, 14, 15). The radioactivities of the injected solutions varied from 0.87 mCi/ml to 2.95 mCi/ml with 84 to >90% of the radioactivity being associated with the cholesterol band by instant thin layer chromatography (ITLC) (see section on chromatography methods).

Preparation of Mice

The mice were anesthetized with diabutal 0.15 mg/g body weight). All tissues were fixed with 5% cacodylate (0.06 M)-buffered glutaraldehyde (24°C). The jugular veins were cut to exsanguinate the animals, the skull was elevated, and the ventral surface of the brain was flooded *in situ* with fixative. The brain was removed and put into fresh glutaraldehyde while the sciatic nerves were exposed and fixed *in situ*. The lateral olfactory stria, the trapezoid body, and the sciatic nerves were dissected, rinsed in saline to remove free radioactive blood, and placed in fresh fixative for 1 h. Pieces of pons, brachial plexus, and trigeminal nerves were rinsed in saline, blotted on filter paper to remove free blood, weighed, and frozen on dry ice for determination of tissue radioactivities. Other weighed pieces of pons were processed in a manner similar to the tissues for autoradiography, using 1 ml of each solution at each step. The radioactivities in each solution and the homogenized GACH-infiltrated tissue were measured on duplicate aliquots.

Determination of Tissue-Specific Activities

The weighed frozen tissues (5 80 mg) were homogenized in ground-glass homogenizers with 0.5 ml saline, and aliquots were counted in Aquasol (New England Nuclear) with the aid of a Packard Tricarb Liquid Scintillation Spectrometer model no. 3375 (Packard Instrument Co., Inc., Downers Grove, Ill.). Quench correction was achieved with an external standard. Tissues with less than 10^3 dpm/mg 1 h or more after injection were not used for autoradiography.

Preparation of GACH

The GACH was prepared as described by Heckman and Barrnett (13). *Cold* carbohydrazide (Polysciences, Inc., Warrington, Pa.), 150 mg/ml of 50% glutaraldehyde, was added slowly to 50% neutralized cold glutaraldehyde (Fisher Scientific Co., Pittsburgh, Pa.) at 0°C in a salt-ice bath with vigorous stirring (13), resulting in a very viscous clear solution. The purity of the carbohydrazide is important; many early batches of GACH failed, i.e. the carbohydrazide would not dissolve in the glutaraldehyde, presumably because of the impurities in the carbohydrazide. The glutaraldehyde was neutralized by stirring vigorously with barium carbonate (1 g/100 ml glutaraldehyde), filtering through Whatman no. 3 paper, and adjusting to pH 7.0 with 0.1 N NaOH. The GACH was poured into cold, disposable syringes and stored at −30°C for up to 4 wk.

Tissue Preparation

The tissues were cut into very small pieces (<0.5 mm thick), maintaining the longitudinal orientation of the myelinated fibers. The tissue fragments were rinsed in buffered sucrose (Sabatini et al., reference 31) for 30 min, postfixed in Dalton's chrome-osmium (DCO) for 1 h, rinsed again in Sabatini's solution for 15 min, and stained en bloc in uranyl acetate (0.25% in 0.1 M acetate buffer) for 1 h, all at room temperature. They were rinsed in cold, glass-distilled water for 15 min and placed in 20% GACH in distilled water overnight at 4°C. Subsequent

infiltration steps were carried out at 4°C with continuous agitation; i.e., 50% GACH 2 h, 80% GACH 4 h, and 100% GACH 1 h. The infiltrated tissue blocks were placed on a flat latex surface in a tiny (approximately 0.1 ml) droplet of fresh 100% GACH and kept in a 37°C oven overnight. The polymerized droplets were oriented and embedded in Epon-Araldite to facilitate sectioning. 1-μm thick sections including the Epon-Araldite collar were stained with toluidine blue (0.2% in 0.5% sodium borate) or paragon multiple stain (Paragon C & C Co., Inc., Bronx, N. Y.) for orientation. Sections were cut on a Porter-Blum MT-2B ultramicrotome (DuPont Instruments, Sorvall Operations, Newtown, Conn.) with 38° glass knives. 1-μm sections were used for light autoradiography, and dark-gold interference color sections (approximately 100 nm as measured by interferometry, see Table I) for electron microscope autoradiography. The section thickness of GACH was determined by cutting a series of sections of GACH-embedded mouse olfactory tract with different interference colors onto glass slides and measuring their thickness with a Varian A-Scope Multiple Beam Interferometer (Varian Associates, Palo Alto, Calif.) after coating the slides and sections with a thin layer of aluminum.

Chromatography

GACH-infiltrated brain homogenate was extracted with $CHCl_3$:MeOH 2:1 and chromatographed on ITLC type silica gel strips (Gelman Instrument Co., Ann Arbor, Mich.), previously activated at 110°C for 30 min, using benzene:ethyl acetate 99:1 as solvent. Standards used for R_f identification were cholesterol, [^{3}H]cholesterol-osmate (ITLC purified [1,2-^{3}H]cholesterol mixed with osmium tetroxide and extracted with $CHCl_3$:MeOH 2:1 [17]) and [^{3}H]cholesterol-osmate suspended in 80% GACH for 4 h and subsequently extracted with $CHCl_3$:MeOH 2:1.

TABLE I

Relationship between Interference Color and Thickness of GACH Sections Compared to Epon Sections (23)

Interference color	Thickness*	
	GACH	Epoxy (23)
	nm	
Gray	40–50	60
Silver	50–60	60–90
Light gold	80–90	90–110
Dark gold	105–115	110–150
Purple	120–130	150–190
Blue	130–145	190–240
Green	180–190	240–280

* The thickness was measured using a filar eye piece to join up the broken lines in a Varian A-Scope Multiple Beam Interferometer.

In each experiment the remainder of the brain was homogenized and extracted by the method of Folch et al. (8) and chromatographed on ITLC against a cholesterol standard. In all instances the spots were revealed by exposure to iodine vapor. The glutaraldehyde fixative used for the tissues 2 h after injection of the cholesterol was extracted and chromatographed as above.

ITLC strips were cut into 1-cm sections and counted in Aquasol. The distribution of radioactivity was compared to the visible standards. All chromatographs were run in duplicate.

Preparation of Autoradiographs

LIGHT MICROSCOPIC AUTORADIOGRAPHY: 1-μm thick carbon- or collodion-coated sections mounted on glass slides were dipped in Ilford L4 emulsion (Ilford Ltd., Ilford, Essex, England) diluted 1:2 and stored at 4°C for estimation of exposure time needed to obtain electron microscope autoradiographs. Severe latent image fading related to the tissue but not to GACH was eliminated by using the same dilution of emulsion as a stripping film (45) and exposing at −20 to −30°C.

ELECTRON MICROSCOPE AUTORADIOGRAPHY: Dark-gold sections perpendicular to the olfactory and trapezoid tracts and parallel to the sciatic nerve from one block from each tissue were picked up on carbon-collodion-coated, 200-mesh grids with handles. The handles were affixed to glass slides with double-stick tape, and a thin layer of carbon was evaporated onto them to prevent potential latent, image fading (negative chemography) (30, 32, 33).

The emulsion was prepared as a stripping film (45). Ilford L4 emulsion was melted and diluted approximately 1:3 with glass-distilled water until purple interference colors were produced on a collodion-coated slide (32). The purple area was outlined and stripped onto glass-distilled water under a yellow safelight (OA-type, Eastman Kodak Co., Rochester, N. Y.). The background was checked before use. The grids were placed section side down on the floating emulsion and picked up on Parafilm (American Can Co., Needham, Mass.) from above. The Parafilm strips were attached to slides with double-stick tape and stored on their sides in light-tight boxes with Humicaps (Driaire Inc., East Norwalk, Conn.), at −20°C for 5–14 mo. Emulsion-coated sections from uninjected littermates and light-exposed sections were included in each box to check for positive and negative chemography, respectively.

After exposure, the grids were brought to room temperature, immersed in amyl acetate with gentle agitation for 4 min to remove the collodion film, and then air dried. The grids were developed with gold latensification (4 min), Elon ascorbic acid (5 min) (gold-EA), at room temperature as described by Salpeter et al. (32, 35) and Rogers (30), rinsed in water, and fixed in Edwal Quick-Fix (Edwal Scientific Products Corp., Chicago, Ill.) diluted 1:5 for 2 min. After washing in distilled water, the grids were stained in 1% uranyl acetate in 70%

acetone for 2 min followed by 0.2% lead citrate for 2 min (29). The grids were processed in forceps individually, in a Ribas staining chamber[1], or most easily with handles inserted into wax-coated slides (41). The grids were examined in a Philips EM-300 electron microscope equipped with a 35-mm camera.

ANALYSES

The distributions of radioactivity in the tissues were determined by silver grain density analysis as described previously and outlined below (2, 15). The half-distance (HD) determined by Salpeter et al. (33–35) for the electron microscope autoradiography specimens used in this study, i.e. ~100 nm sections, Ilford L4 (purple interference color), gold-EA development, is 145 nm. A lattice of uniformly spaced points was superimposed on each micrograph. A transparent overlay with concentric circles marked on it was used to measure the distances of the points and grain centers from predetermined structures. The grain (silver filament) center was taken as the center of the smallest circle which would fully enclose that grain (33).

Micrographs of olfactory tracts and trapezoid bodies were analyzed at × 15,600 (2 h) with a 2 × 2-cm lattice or at × 31,000 (24 h and 6 wk) with a 4 × 4-cm lattice and concentric circles 2.5, 5, 7.5, 10, 12.5, and 15 mm in radius, i.e., approximately 0.5 HD up to 3 HD. Sciatic nerve micrographs were analyzed at × 20,000 with a 2 × 2-cm lattice and circles 3, 6 and 9 mm in radius (i.e., 1, 2, and 3 HD). Background grain density was determined from a minimum of four nonsection micrographs per grid.

Grain densities were obtained by dividing the number of grains by the number of lattice points within a compartment. The standard deviation for each compartment was estimated from the formula $G/P\ [(1/\sqrt{G})^2 + (1/\sqrt{P})^2]^{1/2}$ where G = number of grains and P = number of lattice points (2, 15, 32–34). Before normalization for comparison with standard distribution curves, the background grain density was subtracted from each compartment. The micrographs and tissue compartments were obtained as given below.

[1] The Ribas (Ladd Research Laboratories, Burlington, Vt.) staining chamber works very well, but extraordinarily thorough washing is required to obtain reproducible results. Several autoradiograms were rendered useless, probably because of fixer contamination of the developer within the chamber.

9-Day Old Mouse (1) 2 h Postinjection

All blood vessels encountered in each of three grids from one block each of the trapezoid and olfactory tracts were recorded and analyzed as described below (approximately 80 micrographs).

ANALYSIS 1: (*a*) Blood Vessel Lumen. Grains and points were measured to the nearest endothelial border. Grains and points within 3 HD of two endothelial borders were recorded separately. Grains and points over red blood cells were recorded without regard to distance from lumen or endothelium. (*b*) Endothelium. Grains and points over endothelial cytoplasm were measured to nearest luminal border. Grains and points within 3 HD of another luminal border were recorded separately. (*c*) Endothelial Nuclei. All grains and points were measured to nearest nuclear border without regard to distance from lumen. (*d*) Neuropil Grains and points outside blood vessels were measured to nearest endothelial basement membrane. (*e*) Other Vascular Cells. Grains and points occurring over other cells within the basement membrane were recorded separately, and they accounted for less than 1% of grains and points counted.

The grain densities were normalized to unity over the endothelial compartment 1 HD from the lumen. 32% of the luminal points were more than 3 HD from an endothelial margin. The endothelial wall thickness averaged 3–4 HD, with 45% of the points being >3 HD (450 nm) from the lumen.

10-Day Old Mice (2) 24 h Postinjection

Micrographs of every third microscope field in each of three grids from one trapezoid body were recorded on 35-mm film (150 frames, × 4,300). Four grids from another trapezoid body were micrographed twice. First, every second microscope field at × 4,300 containing myelinated fibers was recorded (54 frames). Second, every field (× 4,300) containing a nucleus was recorded (30 frames). The grids from two nonradioactive trapezoid bodies were also examined. The micrographs were used to examine the distribution of radioactivity relative to myelin sheaths, and the distribution of radioactivity in neurons and glial cells relative to their cytoplasm, nuclei, and adjacent neuropil (Analysis 2).

ANALYSIS 2: The compartments used were: (*a*) Axon (Myelinated Axon). All grains and points over an axon were measured to the nearest inner edge of myelin sheath. (*b*) Myelin Sheaths. All

grains and points. (*c*) Neuronal Nucleus. Grains and points >450 nm from nearest myelin sheath. (*d*) Neuronal Cytoplasm. As for (*c*). (*e*) Glial Nucleus. As for (*c*). (*f*) Glial Cytoplasm. As for (*c*). (*g*) Blood Vessels. Grains and points over lumen and wall were recorded separately, regardless of distance from a myelin sheath. Blood vessels in one olfactory tract were analyzed as in Analysis 1. (*h*) Neuropil. Including unmyelinated axons, dendrites, synapses, glial cell processes, etc., as for (c).

The grains and points in the above mentioned compartments *c*, *d*, *e*, *f* and *h* were further subdivided as follows: (*a*) Neuropil. >450 nm from myelin sheath, neuron and glial cell. (*b*) Neuropil. Within 450 nm of neuronal cytoplasmic border. (*c*) Neuronal Cytoplasm. 0–450 and >450 nm from outer cytoplasmic border. (*d*) Neuronal Nucleus. 0–300 and >300 nm from nuclear membrane. (*e*) Neuropil. Within 450 nm of glial cell border. (*f*) Glial Cytoplasm. 0–300 and >300 nm from cytoplasmic border. (*g*) Glial Nucleus. 0–450 and >450 nm from nuclear border.

Olfactory Tracts and Trapezoid Bodies from 7-wk Old Mice 6 wk Postinjection (two Radioactive and one Control)

Three analyses were performed utilizing (*a*) random micrographs (with respect to tissue sections), (*b*) the random micrographs augmented with micrographs of cells adjacent to the olfactory tracts, and (*c*) the random micrographs augmented with micrographs of myelin sheaths approximately 450 nm (3 HD) thick in trapezoid bodies.

ANALYSIS 3: 26–75 micrographs including every third microscopic field of three to five grids from one block of each olfactory tract and each trapezoid body were used to determine the distribution of label relative to myelin sheaths. The following tissue compartments were recognized: (*a*) Myelin Sheath. Grains and points falling on a myelin sheath (grains and points within 450 nm [3 HD] of another myelin sheath were recorded separately). (*b*) Axon. Grains and points over myelinated axons were recorded in two groups 0–150 nm and 150–300 nm from the nearest inner myelin edge. No exclusions were made and only 10 of 184 points were found more than 300 nm from nearest inner edge. (*c*) Neuropil. Grains and points >450 nm from another myelin sheath were recorded as 0–150, 150–300, 300–450, and >450 nm from the nearest outer edge of a myelin sheath. Grains and points within 450 nm of two or more myelin sheaths were recorded separately. 92% of the first 250 myelin sheaths encountered in the autoradiographs of the adult olfactory tract were <150 nm thick and the remainder were <300 nm. 62% of 520 myelin sheaths in the adult trapezoid body were <150 nm thick, 25% between 150 and 300 nm thick, and the remainder were <600 nm. The average axon radius was 225–300 nm. Therefore, in interpreting the results of the autoradiographic analyses, the axon grain densities in the olfactory tracts and trapezoid bodies were compared to those expected from a radioactive annulus going from radius 2 to 3 HD (see references 15, 32–34), and the grain density distributions outside the myelin sheath were compared to those from a band source of half width 0.5 HD (33, 34).

ANALYSIS 4: The random micrographs of the olfactory tracts were augmented with micrographs of the first five unrecorded cell nuclei encountered in each grid to explore the distribution of the radioactive label in relation to neurons and glial cells (predominantly oligodendrocytes). Grains and points less than 450 nm from a myelin sheath outer edge were excluded. The following compartments were recognized: (*a*) Neuron Cytoplasm; (*b*) Neuron Nucleus; (*c*) Glial Cell Cytoplasm; (*d*) Glial Cell Nucleus; (*e*) Neuropil.

ANALYSIS 5: Random micrographs of the trapezoid bodies containing myelin sheaths 400–500 nm thick were augmented with up to five micrographs per grid (12–18 micrographs per tissue) of other myelin sheaths 400–500 nm thick. The distribution of radioactivity across the width of the myelin sheath was determined on sheaths 400–500 nm thick. Grains and points over axons and myelin sheaths were grouped in 75 nm (0.5 HD) increments relative to the nearest inner (axonal) edge of the myelin sheath. The "edge" compartment included grains and points within 75 nm of the myelin inner edge. Grains and points over axons were excluded if they were <450 nm from another myelin edge.

Sciatic Nerves of two Adult Mice 7-wk Old

The distribution of radioactivity in the myelin sheath relative to the node of Ranvier was examined.

ANALYSIS 6: The first five nodes of Ranvier encountered per grid on four and five grids, respectively, from the sciatic nerve of each of two 7-wk old radioactive mice and one littermate mouse were recorded on 35-mm film. Grains and

points more than 450 nm (3 HD) from another myelin sheath edge were assigned to the following compartments: (*a*) Paranodal Myelin. This included myelin sheaths from the node to the cessation of the "peeling." (*b*) Non-nodal Myelin. Non-nodal myelin was the remainder of the myelin sheaths. (*c* Axon. Subdivided into groups 0–150, 150–300, 300–450, and >450 nm from inner edge of myelin sheath. (*d*) Schwann Cell. Subdivided into compartments 0–150, 150–300, 300–450, and >450 nm from outer edge of myelin. (*e*) Extra Schwann Cell (includes extracellular space, fibroblasts and collagen). Grains and points which were more than 450 nm (3 HD) from a Schwann cell margin or a myelin sheath edge.

RESULTS

Morphology

General tissue preservation was excellent as seen in Figs. 1–5. Neurotubules and filaments are prominent. The myelin periodicity is larger (14.7 ± 0.1 nm) than in conventional epoxy sections (12.3 ± 0.1 nm).[2] Occasional cracks in the sections occurring along cell boundaries are the most obvious clue that the micrographs are from GACH-embedded and not epoxy-embedded tissues. Removal of the collodion support films rendered some of the preparations unstable. With double staining, the contrast in the autoradiographs was excellent. Thin sections were easier to obtain than thick sections.

The distribution of radioactivity recovered from processing solutions and infiltrated brain tissue is shown in Table II. 24 h and 6 wk after injection, >94% of recovered radioactivity is in the infiltrated tissues. The recoveries in these two instances ranged from 60 to 114% of our estimated starting amount. No leaching of radioactivity occurred from the polymerized GACH-embedded tissues into the Epon-Araldite used for support.

The radioactivity (disintegrations/min per milligram tissue) of peripheral nerve was always higher than that of the central nervous tissues: 6×10^3 dpm/mg pons vs. 4×10^4 dpm/mg nerve at 24 h and 2.5×10^4 dpm/mg pons vs. 8×10^4 dpm/mg nerve at 6 wk postinjection. The pons of the littermate control for the 6-wk old mice was also radioactive (5×10^2 dpm/mg).[3]

Chromatography

18–25% of the radioactivity in the GACH-infiltrated tissues ran with the free cholesterol, but the remainder of the radioactivity tended to smear out adjacent to cholesterol-osmate and cholesterol-osmate GACH bands which hardly moved from the origin and did not form discrete spots.

At 2 h, 24 h, and 6 wk postinjection, 58%, 75%–82%, and >90% of ^{3}H in the glutaraldehyde-fixed brain was in the cholesterol band, with the remainder at and just above the origin.

The chromatograms of the $CHCl_3$:MeOH extract of the primary glutaraldehyde fixative 2 h after injection revealed 54% of the radioactivity in the cholesterol band and 28% in the nonpolar region. Recovery of radioactivity applied to the chromatograms was 95% or more.

Electron Microscope Autoradiography

No latent image fading or positive chemography was detected with the electron microscope.

2 h after intraperitoneal (i.p.) injection of [1,2-^{3}H]cholesterol, radioactivity was limited to vascular endothelium (0.37 ± 0.05) and lumen (0.58 ± 0.10) (Fig. 6). Grain density over the neuropil was within 2 SD of the expected distribution from the lumen. Red blood cells and endothelial nuclei were not significantly labeled.

24 h after injection, the endothelium was more labeled than the lumen (Table III). The pattern of endothelial labeling was consistent with that from a uniformly radioactive band 4–6 HD wide corresponding to the average thickness of the endothelium. Myelin sheaths and neuropil were now labeled (differing >3 SD from that expected if the endothelium was the only labeled structure) as were glial and neuronal cytoplasms (Figs. 4, 5, and 7). The grain densities over the axon were not

[2] Hedley-Whyte, E. T., R. F. Lawson, and T. C. Wright. 1974. Quantitative assessment of myelin in GACH-embedded immature and mature mouse brain and nerve. Proceedings of the Seventh International Congress of Neuropathology, Budapest. Akadémiai Kiadó, Budapest. 128.

[3] In a previous study (15), we noticed that the nursing mother's mammary tissue became radioactive. In the present study, we chromatographed a $CHCl_3$:MeOH (2:1) extract of a mother's mammary tissue 24 h after the injection of her suckling pups. The radioactivity was 6×10^3 dpm/mg, of which 88% was in the cholesterol band which was a higher degree of purity than the material administered to the pups.

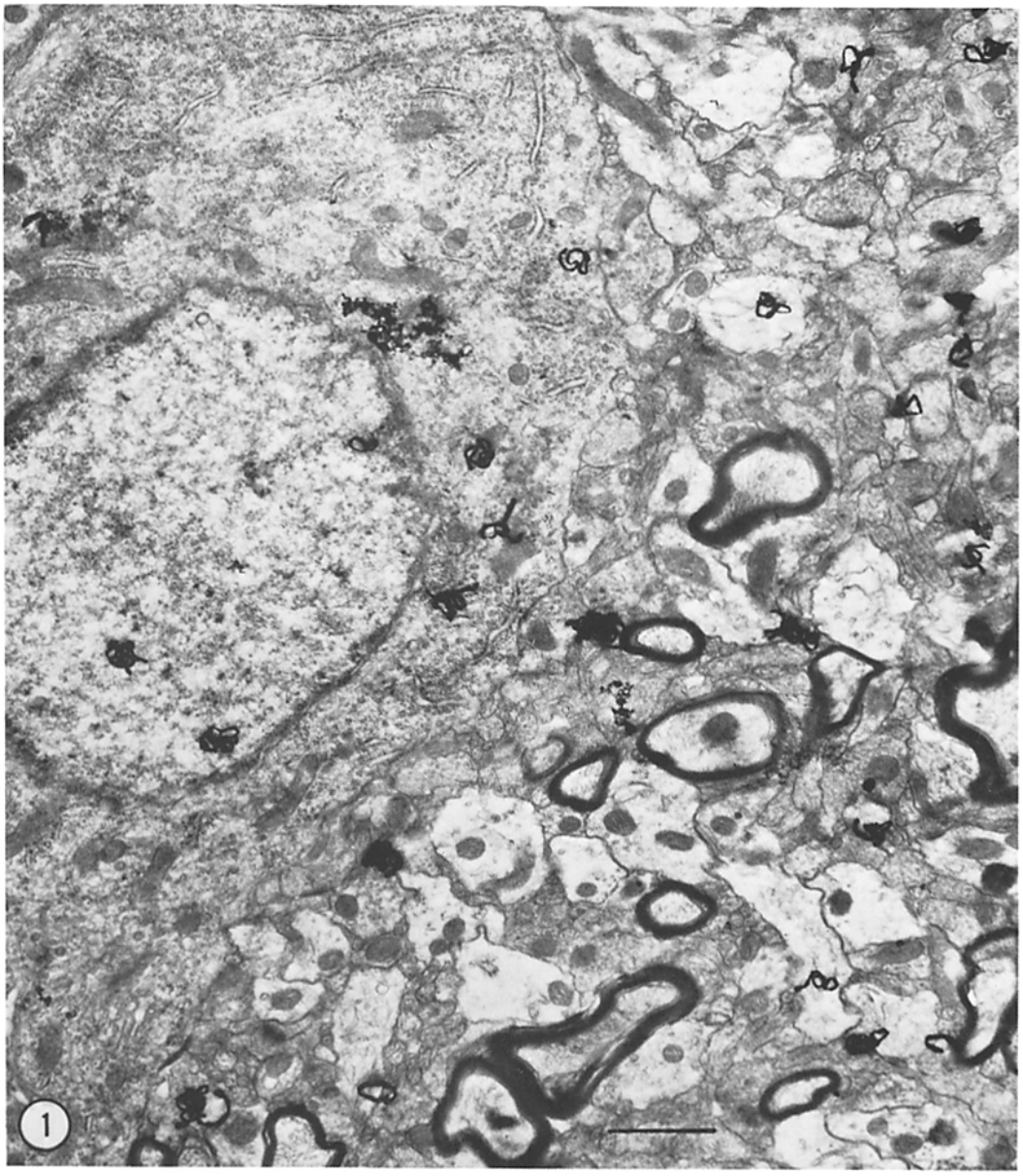

FIGURE 1 Autoradiograph of the olfactory tract and adjacent nucleus of a 7-wk old mouse injected with [1,2-^{3}H]cholesterol at 8, 10, and 12 days. Note the general state of preservation, the prominent Nissl substance in the neuron (left), and the silver grains over the neuron and neuropil. Exposed 7 mo. The marker on all figures is 1 μm. $\times$ 14,500.

significantly different from the expected grain density distribution if all the activity was due to the myelin sheath.

We wished to determine (*a*) whether radioactivity in neuropil was coming from neuronal and/or glial labeling; or (*b*) whether neuronal and glial grain density was attributable to label in the neuropil. Neuronal and glial cytoplasm and neuronal nucleus were more labeled than could be accounted for by radioactivity in the neuropil, but

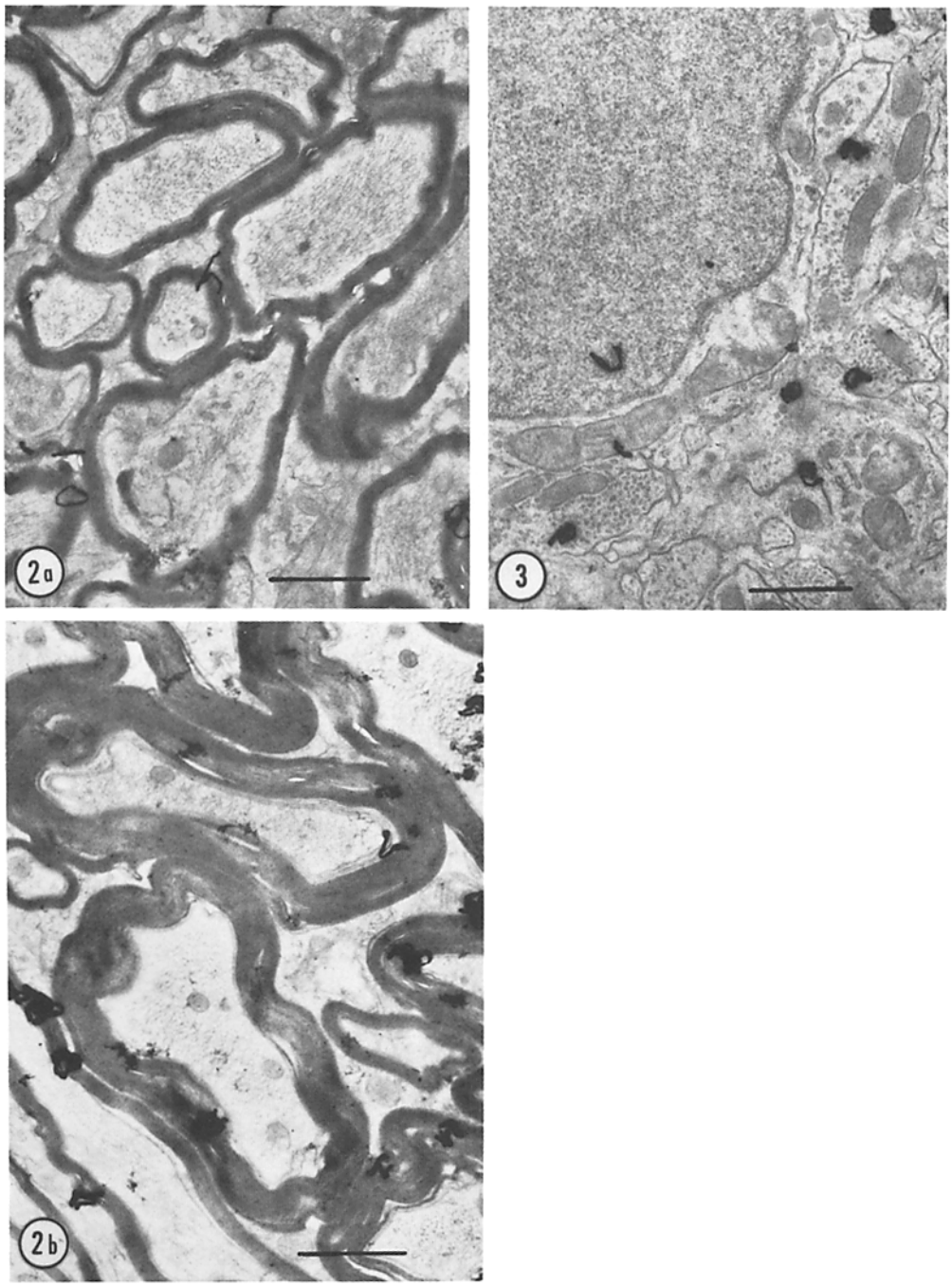

FIGURE 2 *a* Autoradiograph of olfactory tract of a 7-wk old mouse injected with [1,2-^{3}H]cholesterol at 8, 10, and 12 days of age. Note thickness of myelin sheaths and lack of intermyelinated fiber space. Exposed 7 mo. × 13,800.

FIGURE 2 *b* Autoradiograph of the trapezoid body from a 7-wk old mouse injected at 8, 10, and 12 days with [1,2-^{3}H]cholesterol. Note silver grains over myelin sheaths, prominent neurofilaments in axons, and close packing of the myelinated fibers. Exposure 7 mo. × 15,000.

FIGURE 3 Autoradiograph of olfactory tract of a 10-day old mouse 24 h after injection of [1,2-^{3}H]cholesterol. Note label over glial cell (probable oligodendrocyte) and neuropil. Exposed 11 mo. × 13,800.

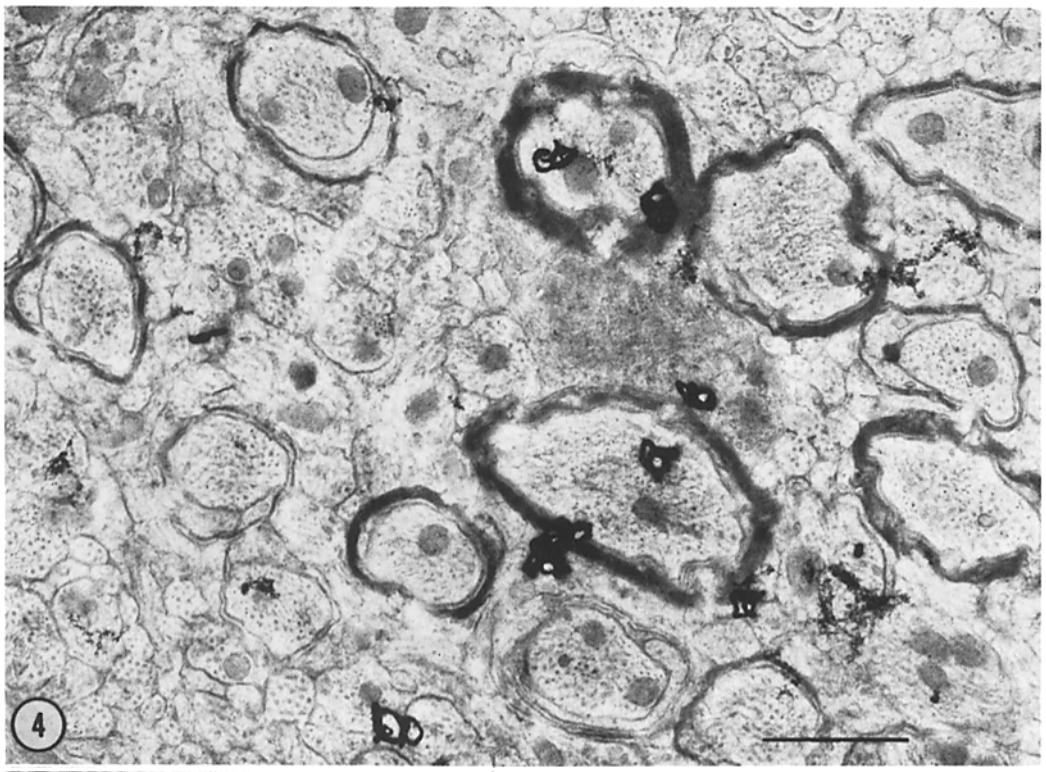

FIGURE 4 Autoradiograph of the trapezoid body of a 10-day old mouse 24 h after injection of [1,2-^{3}H]cholesterol. Note myelinating fibers and silver grains over myelinated fibers and neuropil. Exposure 11 mo. × 18,500.

FIGURE 5 Autoradiograph of a capillary in the olfactory tract of a 10-day old mouse 24 h after injection of [1,2-^{3}H]cholesterol, showing silver grains over endothelial cells, capillary lumen, and platelets. Exposure 14 mo. × 7,200.

TABLE II

The Fate of [1,2-^{3}H]Cholesterol during Processing of Mouse Brain into GACH at 2 h, 24 h, and 6 wk after Injection into Suckling Mice

Processing solutions	Recovered radioactivity*		
	2 h (7)‡	24 h (6)	6 wk (4)
		% ± *SD*	
Glutaraldehyde	12.0 ± 5.0	6.0 ± 2.0	0.05 ± 0.05
Washing solutions and Dalton's chrome osmium	5.0 ± 1.0	0.7 ± 0.5	1.8 ± 0.8
20–100% GACH (pooled)	1.5 ± 1.0	0.3 ± 0.2	0.15 ± 0.04
Infiltrated tissue	81.0 ± 7.0	94.0 ± 2.0	98.0 ± 1.0

* Recovered radioactivity ranged from 26 to 138% of calculated starting amounts based on scintillation counting of homogenized, weighed fresh tissue. Two sources of variation were the use of wet weights of small pieces of tissue and the failure to rinse the tissue fragments in saline before homogenization in the early experiments.
‡Number of samples.

TABLE III

Distribution of Radioactivity Relative to Cerebral Blood Vessels of 10-Day Old Mice 24 h after Injection of [1,2-^{3}H]Cholesterol

Tissue compartment*		Expected grain density distribution if endothelium was uniformly labeled‡	Grain density per unit area ± SD§ normalized to unity over inner endothelial compartment
	nm		
Lumen	>450	<0.10	0.24 ± 0.03‖
	300–450	0.18	0.30 ± 0.10
	150–300	0.30	0.77 ± 0.27
	0–150	0.50	0.67 ± 0.17
Endothelium	0–150	1.00	1.00 ± 0.25
	150–300	1.54	1.58 ± 0.46
	300–450	1.20	1.22 ± 0.33
	>450	1.00	0.90 ± 0.12
Neuropil	0–150	0.50	0.78 ± 0.24
	150–300	0.30	0.64 ± 0.19
	300–450	0.18	0.34 ± 0.11
	>450	<0.10	0.22 ± 0.02‖

* Details of analysis are same as 2 h after injection, Analysis 1.
‡ cf. distribution around a solid band 3 HD in half width reference 33.
‖ Differs by >3 SD from expected density.
§ 1,112 grains and 732 points were counted.

the neuronal nuclear label was within 2 SD of that expected from the vascular label. The glial nucleus was not significantly different from that expected if the label was from neuropil (Table IV).

Fig. 8 shows the means ± SEM for the grain densities normalized to unity over myelin for the combined data from the adult olfactory and trapezoid tracts. The grain density per unit area over the axon was not significantly different from that expected if the myelin sheaths were the only source of radioactivity. The grain density distribution outside the myelinated fibers was clearly different from the theoretical curve, and its variations among tissue elements of the olfactory tracts is shown in more detail in Fig. 9. All elements except for the glial nuclei appeared to be labeled. No

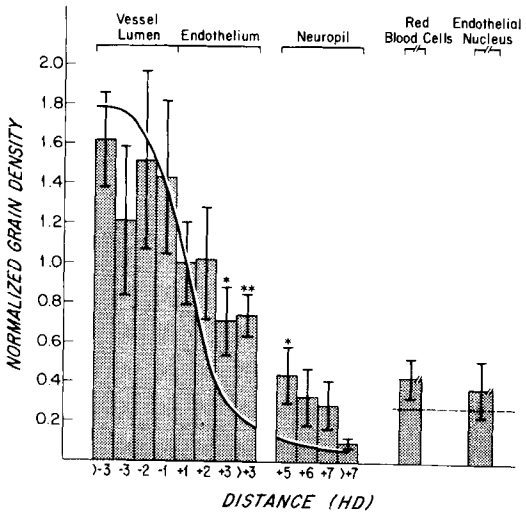

FIGURE 6 Distribution of radioactivity (grain density ± SD) in trapezoid body and olfactory tract of one 9-day old mouse 2 h after injection of [1,2-^{3}H]cholesterol. Grain density was normalized to unity over the endothelium within 1 HD of the vessel lumen. Grains and points over the lumen and endothelial cells were measured to the nearest luminal endothelial membrane more than 450 nm (3 HD) from another luminal endothelial membrane. Grains and points over the neuropil were measured to the nearest abluminal endothelial membrane. No grains or points were excluded from the neuropil, endothelial nucleus, or red blood cell compartments. The smooth curve superimposed on the histogram is the theoretical distribution of radioactivity from a uniformly labeled band source 8 HD in width (cf. curve labeled 4 HD, reference 32). The interrupted line represents the integrated expected grain densities from 1 to 4 HD from a band source 8 HD in width. Note that the grain density over the lumen is consistent with a uniformly labeled band source. The endothelial cells were more labeled, > 2 SD (*), or 3 SD (**), than would be expected if radioactivity were limited to the lumen. The grain density over the neuropil could be accounted for by the endothelial radioactivity. No significant labeling was detected in red blood cells or endothelial nuclei. Grain densities over endothelial nuclei more than 450 nm (3 HD) from the nuclear membrane were within 1 SD of background. 810 grains and 6,545 points were included in the analysis. Occasional vessels had pericytes whose grain density could be accounted for by endothelial labeling.

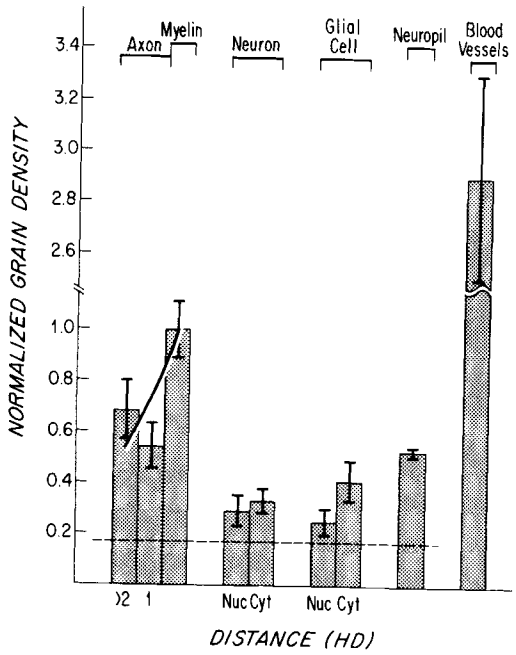

FIGURE 7 Distribution of radioactivity (grain density ± SD) normalized to unity over myelin in the trapezoid bodies of two 10-day old mice 24 h after injection of [1,2-^{3}H]cholesterol. All grains and points were included in axon and myelin compartments. Grains and points within 3 HD of a myelin sheath were excluded from the neuronal, glial cell, and neuropil compartments. The solid line is the expected grain density over the axon if all axonal label were from myelin (see Fig. 8). The interrupted line represents the expected grain density around the blood vessels considered as a disk 4 HD in average radius and an average 7 HD away from such a disk (see reference 33). Note high level of labeling of blood vessels compared to that of myelin. Neuropil, neuronal, and glial cytoplasm are all labeled (>3 SD) more than can be attributed to blood vessel and myelin radioactivity. Axon labeling is within 2 SD of the expected distribution of myelin. 56% of axon area was within 1 HD of a myelin inner edge, 30% between 1-2 HD, and 14% between 2-3 HD. 1,178 grains and 5,559 points were counted. *Nuc* = nucleus, *Cyt* = cytoplasm.

significant differences in grain density were found for synapses, dendrites, and remaining neuropil.

The distribution of [1,2-^{3}H]cholesterol within those myelin sheaths 450 nm wide (3 HD) was not statistically different from that expected of a 3 HD wide radioactive band (Table V). The axons within those same sheaths (average radius 3 HD) were not labeled more than could be accounted for by the myelin radioactivity.

Table VI gives the relative proportion of grains and area analyzed for each compartment of the central nervous system.

The distribution of [1,2-^{3}H]cholesterol in the sciatic nerves of two adult mice is seen in Figs. 10

TABLE IV

Distribution of Radioactivity in Neurons and Glial Cells of Trapezoid Bodies of Two 10-Day old Mice 24 h after Injection of [1,2-^{3}H]Cholesterol

Tissue compartment	Grain density per unit area ± SD		
	Measured	Normalized to unity over neuropil	Expected density* assuming radioactivity limited to neuropil
(*a*) Neuropil >450 nm from cell border	0.19 ± 0.01‡	1.00 ± 0.05	1.00
(*b*) Neuropil 0–450 nm from neuron	0.18 ± 0.05	0.97 ± 0.28	
(*c*) Neuron cytoplasm 0–450 nm	0.13 ± 0.04	0.70 ± 0.23	~0.40
>450 nm	0.11 ± 0.02	0.58 ± 0.12§	<0.20
(*d*) Neuron nucleus 0–300 nm	No compartment		
>300 nm	0.09 ± 0.02	0.48 ± 0.12§	<0.20
(*e*) Neuropil 0–450 nm from glial cell	0.16 ± 0.04	0.83 ± 0.23	
(*f*) Glial cytoplasm 0–300 nm	0.13 ± 0.04	0.68 ± 0.23	~0.50
>300 nm	0.15 ± 0.04	0.81 ± 0.22§	<0.30
(*g*) Glial nucleus 0–450 nm	0.24 ± 0.11	1.24 ± 0.58	
>450 nm	0.08 ± 0.02	0.40 ± 0.10	<0.20

* Assumes neuropil to be a solid band of infinite thickness (33, 34).

‡ If all the radioactivity was limited to the blood vessels the expected measured activity would be 0.08, assuming that blood vessels are radioactive disks approximately 4 HD in radius and mostly >8 HD away from the cells. If the radioactivity were all from myelin as an annulus of inner and outer radii 2 HD and 3 HD, the expected measured grain density >3 HD from myelin was 0.02.

§ Differs by >2 SD from expected density.

and 11. The Schwann cells and axons were labeled to a significantly greater extent than could be accounted for by radioactivity limited to myelin. The grain density of the extra-Schwann cell compartment, including fibroblasts and C fibers, was not significantly different from the density expected if myelin were the only structure labeled. In both animals, the non-nodal myelin had a higher grain density (0.62 ± 0.03) than the paranodal (0.53 ± 0.05).

DISCUSSION

Cholesterol and Myelin Stability

[1,2-^{3}H]Cholesterol incorporated into the central nervous system during myelination is not limited to myelin sheaths in the adult brain. Myelin sheaths are the most heavily labeled structures; however, 18–46% of the grains counted in the adult brain were not related to myelinated fibers. Despite marked radioactivity in mature neuropil which contains many unmyelinated axons as well as dendrites and glial cell processes, we were unable to demonstrate label in the axons of myelinated fibers beyond that which could be attributed to the radioactive myelin sheaths. The finding of radioactivity within neuronal cell bodies and dendrites, as well as the neuropil, had predicted that there should be some labeled cholesterol within the axons as well.

Subsequent to the classical descriptions of the stability of cholesterol incorporated into the nervous system during development, as reported by Davison et al. (5, 6), many investigators have confirmed the observations and attempted to explore the localization of such cholesterol (1, 7, 9, 10, 14–16, 20, 25–28, 40, 43). The presence of stable cholesterol had been interpreted as indicating persistence of that cholesterol in the myelin sheath. This interpretation viewed the spiral formation of myelin (11) as resulting in an inert structure (44). More recently, Spohn and Davison (40) have reported uniform specific activities of cholesterol in all brain subcellular fractions 21 days after injection into 16-day old rats, and Banik and Davison (1) have shown that cholesterol

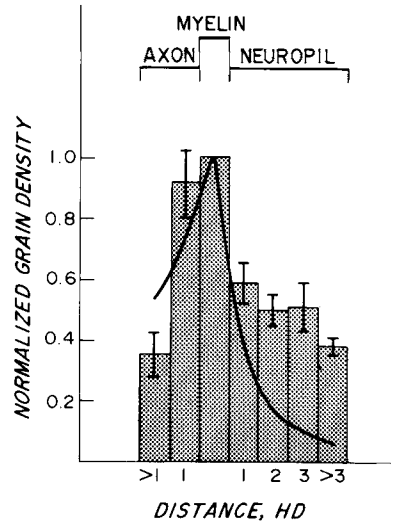

FIGURE 8 Distribution of radioactivity (grain density ± SEM) in the olfactory tracts and trapezoid bodies of two 7-wk old mice injected three times with [1,2-^{3}H]cholesterol at 8, 10, and 12 days of age. The grain densities have been normalized to one over myelin, and each compartment is expressed as the mean ± SEM of four observations except for neuropil 3 HD which is mean ± SEM of three observations. All grains and points over the axons were included in the analysis but grains and points <3 HD from another myelin sheath were excluded from the myelin and neuropil compartments. The theoretical curve superimposed on the histogram is based on the assumption for the axon of a radioactive annulus going from radius 2 HD to 3 HD and a radioactive band 1 HD thick for the neuropil (15, 32–34). Note that the neuropil labeling clearly exceeds (>4 SE or 2 SD) the expected density, indicating that [1,2-^{3}H]cholesterol is also present in the neuropil. The level of label detected in the axon is within 2 SE of the theoretical distribution if all activity were attributable to myelin. 1,500 grains and 4,915 points were counted.

readily exchanges between myelin and microsomes in the young rat brain. In the current study, the [1,2-^{3}H]cholesterol incorporated into the brain during development remained within the brain in myelin sheaths, neuropil, neurons, and glial cells.

Other evidence for an internal recirculation of cholesterol within the central nervous system has come from experiments utilizing intraventricular injection of [^{14}C]mevalonic acid into adult rats (36, 37). Cholesterol formed in the brain appeared to be exchanged between subcellular structures as well as between brain and plasma (36). Evidence for a similar exchange of [^{35}S]cerebroside between microsomes and myelin has also been presented (19). Other authors have also demonstrated exchange and redistribution of labeled myelin constituents in rat brain between microsomes and myelin (19, 25, 36). The presence of [1,2-^{3}H]cholesterol in neuronal nuclei and cytoplasm as well as myelin may be morphologic evidence in support of this idea. 6 wk after injection of [1,2-^{3}H]cholesterol into mice, the only substantial remaining radioactivity is found in the brain (14). Although the mice received a small amount of [1,2-^{3}H]cholesterol via the mother's milk, the amounts were insufficient to show up in autoradiographs of the uninjected littermates.

Entry of Cholesterol into Brain

The most strongly labeled structures in the brain 2 and 24 h postinjection were the blood vessels. 2 h after injection, the [1,2-^{3}H] cholesterol was effectively limited to the lumen and the endothelium. At 24 h after injection, although the endothelium was the most labeled structure, label was also detectable in myelin sheaths, neuronal and glial cytoplasm, and neuropil. The grain density observed for the axons could be accounted for by the label in the myelin sheaths. The affinity of [1,2-^{3}H]cholesterol for endothelial cells in the immature and mature mouse is being further investigated. It is interesting to note that red blood cells were not

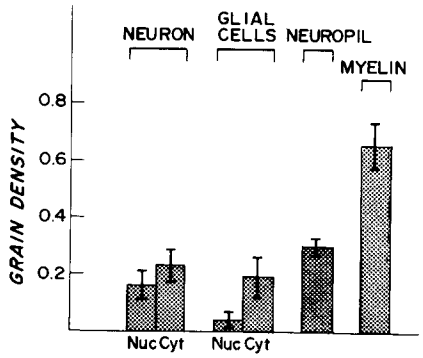

FIGURE 9 Distribution of radioactivity (grain density ± SD) in neuropil of olfactory tracts of two mice 6 wk after injection of [1,2-^{3}H]cholesterol at 8, 10, and 12 days of age. The grain density for myelin is given for comparison. Only grains and points more than 3 HD from myelin were included in these analyses. Glial nuclear labeling is not significantly different from background. Otherwise the label is found in all parts of the neuropil. *Nuc* = nucleus, *Cyt* = cytoplasm.

TABLE V

Distribution of [1,2-^{3}H]Cholesterol in Myelin Sheaths 3 HD Width and Their Axons in Two Adult Trapezoid Bodies 6 wk Postinjection

Compartment	HD	Grain density per unit area ± SD		
		Measured	Normalized to unity over edge compartment	Expected if radioactivity limited to a band 3HD wide (33, 34)
Into axon*	−3.5‡	0.09 ± 0.07	0.46 ± 0.32	0.16
	−2.5	0.12 ± 0.07	0.61 ± 0.36	0.20
	−1.5	0.26 ± 0.10	1.28 ± 0.51	0.35
	−0.5	0.37 ± 0.13	1.79 ± 0.66	0.80
Myelin edge		0.22 ± 0.08	1.00 ± 0.34	1.00
Into myelin sheath§	+0.5‖	0.49 ± 0.20	2.59 ± 0.92	1.25
	+1.5	0.82 ± 0.36	1.54 ± 0.43	1.50
	+2.5	0.26 ± 0.13	1.70 ± 0.38	1.25

Total number of grains 700 and points 2,720.
* All grains and points over the axon.
‡ Measured from 75 nm inside axon from inner edge of myelin sheath.
§ Grains and points more than 3 HD from another myelin sheath.
‖ Measured from 75 nm outside axon into myelin sheath.

TABLE VI

Percent Distribution of Pooled Grains and Pooled Points for Compartments of the Central Nervous System, 2 h, 24 h, and 6 wk after Injection of [1,2-^{3}H]Cholesterol into Suckling Mice

Compartment	Trapezoid and olfactory*		Trapezoid‡		Olfactory§		Trapezoid§	
	Grains‖	Points‖	Grains	Points	Grains	Points	Grains	Points
Myelin	—	—	9	5	31	16	54	41
Myelinated axon	—	—	8	8	20	16	26	37
Neuropil	33	73	64	70	34	38	18	21
Neuron	—	—	5	9	12	19	—	—
Glial cells	—	—	5	6	3	11	—	—
Blood vessel lumen	21	4	9¶	2¶	—	—	—	—
Endothelium	31	10	—	—	—	—	—	—
Red blood cell	11	7	—	—	—	—	—	—

* 2 h postinjection.
‡ 24 h postinjection.
§ 6 wk postinjection.
‖ Includes grains and points <450 nm from myelin.
¶ Does not include grains and points in Fig. 5 and Table III.

appreciably labeled 2 and 24 h after the injection of [1,2-^{3}H]cholesterol, but platelets when seen 24 h after the injection were highly labeled (Fig. 5). The lack of detectable myelin labeling up to 2 h after injection is in contrast to the case of the sciatic nerve where myelin labeling was detected within 20 min of [1,2-^{3}H]cholesterol injection (26). No comments were made about the vascular labeling in

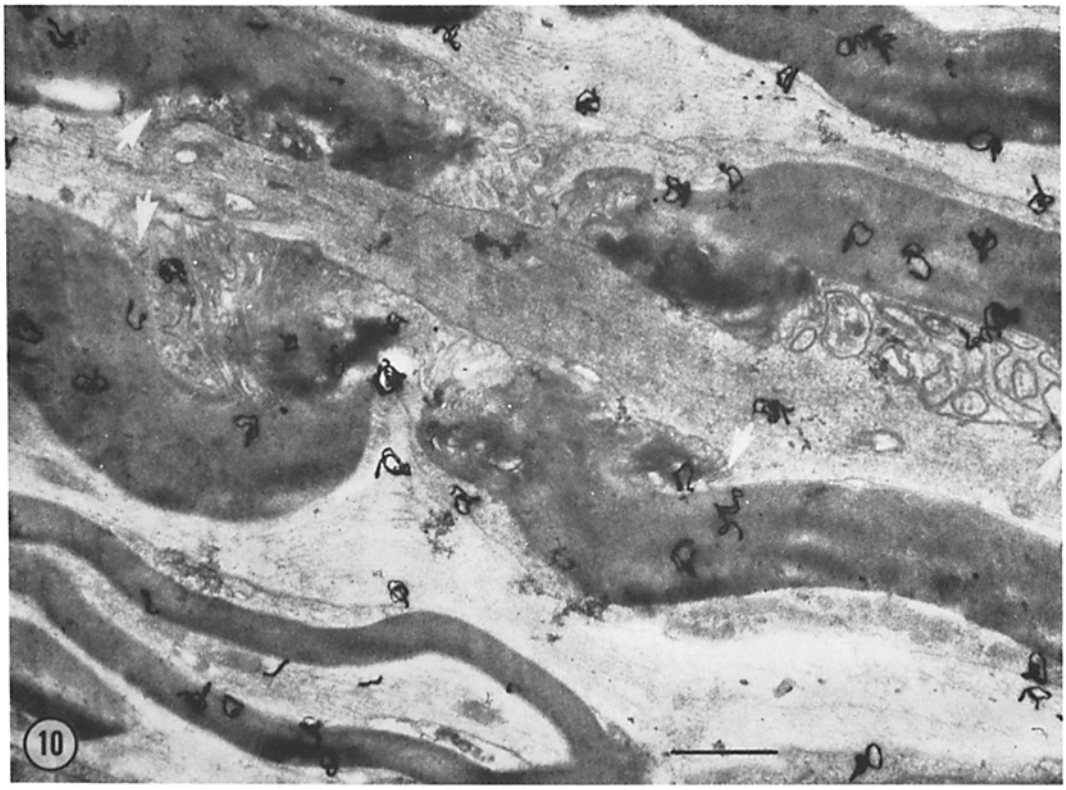

FIGURE 10 Autoradiograph of a node of Ranvier in the sciatic nerve of a 7-wk old mouse injected with [1,2-^{3}H]cholesterol at 8, 10, and 12 days of age. In the analysis, nodal myelin included the myelin sheath from the node to the beginning of the "peeling off" (arrow) of the Schwann cell-myelin membrane. Note marked activity over myelin as well as scattered grains over axons and Schwann cells. Exposure 5 mo. × 13,800.

that study (26). No endothelial labeling was detected 6 wk after injection of [1,2-^{3}H]cholesterol.

Role of Node of Ranvier in Myelin Metabolism

Davison (3) suggested that the metabolic activity of adult myelin might be at nodes of Ranvier or in the axolemma. The slight decrease in grain density over paranodal myelin in this study could be due to the increased amounts of Schwann cell cytoplasm on the inside of the sheath included in this compartment, and does not suggest any differential distribution of cholesterol incorporated early in myelination from that incorporated later on. However, the role, if any, of the node of Ranvier in the incorporation of cholesterol into myelin requires more subtle inquiry and is currently being investigated.

The current observations of the adult sciatic nerves also confirm previous observations made on sciatic nerve with both Epon-Araldite and modified Idelman Epon-Araldite-embedded material (15, 16, 18, 26, 28). The results also reaffirm that shifts in cholesterol distribution in the lung were more a reflection of the method of fixation than of section preparation (2).

Technical Considerations

The morphology of GACH-embedded tissues is markedly improved over that in the modified Idelman method. In the latter the axons are nearly always collapsed and many of the myelin sheaths are distorted (15, 16, 26, 28). Even though Heckman and Barrnett (13) described many small holes in their sections, we did not find them in our autoradiographs of osmium-tetroxide-fixed tissues although they were seen in some initial experiments. The consistent artifact that we observed

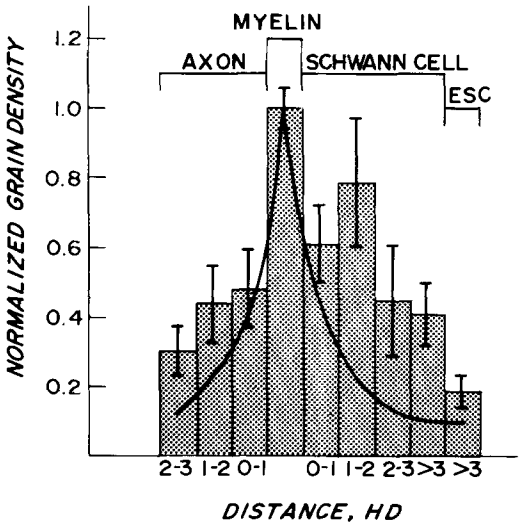

FIGURE 11 Distribution of radioactivity normalized to unity over the myelin sheaths in longitudinal sections of the sciatic nerves of 7-wk old mice (two) injected with [1,2-^{3}H]cholesterol at 8, 10, and 12 days of age. Both axons and Schwann cells are labeled more than (>2 SD from expected) can be accounted for by myelin labeling. Label outside Schwann cells (*ESC*) is compatible with the grain density expected if myelin were the only radioactive source. The myelin compartment includes both nodal and paranodal myelin. Total number of grains 1,376 and points 2,656.

was splitting of sections along cell membranes in a random orientation with respect to the direction of cutting. In these experiments, we used osmium tetroxide because of the improved cytologic contrast and because it does not appear to aggravate cholesterol extraction from the tissue.

The amount of cholesterol found elsewhere than in the infiltrated tissues during processing 6 wk after injection was negligible. The counts found in the initial fixative and washing solutions of tissues obtained 2 h and, to a lesser extent, 24 h after injection probably came from small quantities of highly radioactive plasma and blood which must escape into the solutions around the tissues. In addition, the amount of radioactivity lost into the various solutions from tissues taken 6 wk after injection (<2%) was reproducible, in contrast to Idelman's method (18) in which the loss of [1,2-^{3}H]cholesterol into the processing solutions was highly variable (2, 16).

Certain precautions have to be taken with respect to latent image fading when GACH-embedded nervous tissues are used. Aldehydes are known to cause latent image fading (30), but the fading observed with the light microscope was not related to the GACH but to the tissue. Latent image fading was not a problem with the thin sections or when stripping film was used for the thicker sections (45). There are two possible reasons for this: (*a*) in emulsion-dipped, carbon-coated 1-μm sections, the carbon layer had a cracked appearance and probably allowed contact between tissues and emulsion; and (*b*) the relative bulk of section to carbon layer and emulsion is markedly greater in 1-μm than 100-nm sections. Prior staining with uranyl acetate protected the autoradiographs from the destructive effects of the lead stain (32) and resulted in very high contrast (Fig. 2 *a* and *b*).

The chromatography of the GACH-infiltrated tissues redemonstrated the difficulty of extracting and chromatographing compounds trapped in a rapidly polymerizing substance. Furthermore, cholesterol osmate had a slower R_f than cholesterol, and the R_f value seemed to be further decreased by the addition of glutaraldehyde (12, 13, 17, 21, 22, 46). We therefore feel that the tritium we were looking at in the autoradiographs represents [1,2-^{3}H]cholesterol as discussed previously (14).

The ability to look at nonpolar myelin constituents within the central nervous system, which have not been partially extracted, will allow exploration of the pathway of myelin components from blood vessel to myelin sheath during their incorporation. It will also allow investigation of the fate of previously incorporated water-insoluble molecules during demyelination and also during degeneration and attempts at remyelination within the central nervous system.

I am indebted to Rebecca F. Lawson for superb assistance, criticism, and encouragement. I would also like to acknowledge the inspiration and encouragement of Dr. Betty G. Uzman.

Supported in part by U. S. Public Health Service Program-Project Grant NS09704, HD 06276, and NS10990 from the National Institutes of Health, and by the United Cerebral Palsy Research and Education Foundation.

Received for publication 20 August 1974, and in revised form 4 February 1975.

REFERENCES

1. BANIK, N. L., and A. N. DAVISON. 1971. Exchange of sterols between myelin and other membranes of developing rat brain. *Biochem. J* **122**:751-758.

2. DARRAH, H. K., J. HEDLEY-WHYTE, and E. T. HEDLEY-WHYTE. 1971. Radioautography of cholesterol in lung. An assessment of different tissue processing techniques. *J. Cell Biol.* **49**:345–361.
3. DAVISON, A. N. 1961. Biochemistry and the myelin sheath. *Sci. Basis Med.* 220–235.
4. DAVISON, A. N. 1970. The biochemistry of the myelin sheath. *In* Myelination. A. N. Davison and A. Peters, editors. Charles C. Thomas, Publisher. Springfield, Ill. 80–161.
5. DAVISON, A. N., J. DOBBING, R. S. MORGAN and G. PAYLING-WRIGHT. 1959. Metabolism of myelin. The persistence of (4-^{14}C)cholesterol in the mammalian central nervous system. *Lancet.* **1**:658–660.
6. DAVISON, A. N., and M. WAJDA. 1959. Persistence of cholesterol (4-^{14}C) in the central nervous system. *Nature (Lond.).* **183**:1606–1607.
7. DHOPESHWARKAR, G. A., C. SUBRAMANIAN, and J. F. MEAD. 1971. Rapid uptake of (1-^{14}C) acetate by the adult rat brain 15 seconds after carotid injection. *Biochim. Biophys. Acta.* **248**:41–47.
8. FOLCH, J., M. LEES, and G. H. SLOANE STANLEY. 1957. A simple method for the isolation and purification of total lipides from animal tissues. *J. Biol. Chem.* **226**:497–509.
9. GAUTHERON, C., and F. CHEVALLIER. 1971. Problèmes posés par la radioautographie a haute résolution, du cholesterol tissulaire, cérébral en particulier. *J. Microsc. (Paris).* **10**:99–106.
10. GAUTHERON, C., L. PETIT, and F. CHEVALLIER. 1969. Synthesis of cholesterol into the central nervous system and its radioautographic localization. *Exp. Neurol.* **25**:18–23.
11. GEREN, B. B. 1954. The formation from the Schwann cell surface of myelin in the peripheral nerves of chick embryos. *Exp. Cell Res.* **7**:558–562.
12. GIGG, R., and S. PAYNE. 1969. The reaction of glutaraldehyde with tissue lipids. *Chem. Phys. Lipids.* **3**:292–295.
13. HECKMAN, C. A., and R. J. BARRNETT. 1973. GACH: a water miscible, lipid-retaining embedding polymer for electron microscopy. *J. Ultrastruct. Res.* **42**:156–179.
14. HEDLEY-WHYTE, E. T., H. K. DARRAH, F. STENDLER, and B. G. UZMAN. 1968. The value of cholesterol-1,2-^{3}H as a long term tracer for autoradiographic study of the nervous system of mice. *Lab. Invest.* **19**:526–529.
15. HEDLEY-WHYTE, E. T., F. A. RAWLINS, M. M. SALPETER, and B. G. UZMAN. 1969. Distribution of cholesterol-1,2-^{3}H during maturation of mouse peripheral nerve. *Lab. Invest.* **21**:536–547.
16. HEDLEY-WHYTE, E. T., and B. G. UZMAN. 1968. Comparison of cholesterol extraction from tissues during processing for electron microscopic radioautography. *In* Proceedings of the Electron Microscopy Society of America, 26th Annual Meeting. C. J. Arcenaux, editor. Claitor's Publishing Div., Baton Rouge, La. 92–93.
17. HIGGINS, J. A., N. T. FLORENDO, and R. J. BARRNETT. 1973. Localization of cholesterol in membranes of erythrocyte ghosts. *J. Ultrastruct. Res.* **42**:66–81.
18. IDELMAN S. 1964. Modification de la technique de Luft en vue de la conservation des lipides en microscopie electronique. *J. Microsc. (Paris).* **3**:715–718.
19. JUNGALWALA, F. B. 1974. Synthesis and turnover of cerebroside sulfate of myelin in adult and developing rat brain. *J. Lipid Res.* **15**:114–123.
20. KABARA, J. J. 1965. Brain cholesterol. XI. A review of biosynthesis in adult mice. *J. Am. Oil Chem. Soc.* **42**:1003–1008.
21. KORN, E. D. 1966. Synthesis of bis(methyl 9,10-dihydroxystearate) osmate from methyl oleate and osmium tetroxide under conditions used for fixation of biological material. *Biochim. Biophys. Acta.* **116**:317–324.
22. KORN, E. D. 1967. A chromatographic and spectrophotometric study of the products of the reaction of osmium tetroxide with unsaturated lipids. *J. Cell Biol.* **34**:627–638.
23. PEACHEY, L. D. 1958. Thin sections. I. A study of section thickness and physical distortion produced during microtomy. *J. Biophys. Biochem. Cytol.* **4**:233–242.
24. PEASE, D. C., and R. G. PETERSON. 1972. Polymerizable glutaraldehyde-urea mixtures as polar, water-containing embedding media. *J. Ultrastruct. Res.* **41**:133–159.
25. RAMSEY, R. B., J. P. JONES, and H. J. NICHOLAS. 1972. The biosynthesis of cholesterol and other sterols by brain tissue. *J. Neurochem.* **19**:931–936.
26. RAWLINS, F. A. 1973. A time-sequence autoradiographic study of the in vivo incorporation of 1,2-^{3}H cholesterol into peripheral nerve myelin. *J. Cell Biol.* **58**:42–53.
27. RAWLINS, F. A., and M. E. SMITH. 1971. Myelin synthesis in vitro: a comparative study of central and peripheral nervous tissue. *J. Neurochem.* **18**:1861–1870.
28. RAWLINS, F. A., G. M. VILLEGAS, E. T. HEDLEY-WHYTE, and B. G. UZMAN. 1972. Fine structural localization of cholesterol-1,2-^{3}H in degenerating and regenerating mouse sciatic nerve. *J. Cell Biol.* **52**:615 625.
29. REYNOLDS, E. S. 1963. The use of lead citrate at high pH as an electron-opaque stain in electron microscopy. *J. Cell Biol.* **17**:208–212.
30. ROGERS, A. W. 1973. Techniques of Autoradiography. Elsevier Scientific Publishing Company, Amsterdam. 2nd edition.
31. SABATINI, D. D., K. BENSCH, and R. J. BARRNETT. 1963. Cytochemistry and electron microscopy. The preservation of cellular ultrastructure and enzymatic activity by aldehyde fixation. *J. Cell Biol.* **17**:19–58.

32. SALPETER, M. M., and L. BACHMANN. 1973. Autoradiography. *In* Principles and Techniques of Electron Microscopy. Biological Applications. M. A. Hayat, editor. Van Nostrand Reinhold Company, New York. **2**:221–278.
33. SALPETER, M. M., L. BACHMANN, and E. SALPETER. 1969. Resolution in electron microscope radioautography. *J. Cell Biol.* **41**:1–20.
34. SALPETER, M. M., and F. A. MCHENRY. 1973. Electron microscope autoradiography, analyses of autoradiograms. *In* Advanced Techniques in Biological Electron Microscopy. J. K. Koehler, editor. Springer-Verlag New York Inc., New York. 113–152.
35. SALPETER, M. M., and M. SZABO. 1972. Sensitivity in electron microscope autoradiography. I. The effect of radiation dose. *J. Histochem. Cytochem.* **20**:425–434.
36. SEROUGNE-GAUTHERON, C., and F. CHEVALLIER. 1973. Time course of biosynthetic cholesterol in the adult rat brain. *Biochim. Biophys. Acta.* **316**:244–250.
37. SEROUGNE, C., and F. CHEVALLIER. 1974. Microscopic radioautography of adult rat brain cholesterol. Problem of the blood-brain barrier. *Exp. Neurol.* **44**:1–9.
38. SMITH, M. E. 1967. The metabolism of myelin lipids. *In* Advances in Lipid Research, R. Paoletti and D. Kritchevsky, editors. Academic Press, New York and London. **5**:241–278.
39. SMITH, M. E. 1968. The turnover of myelin in the adult rat. *Biochim. Biophys. Acta.* **164**:285–293.
40. SPOHN, M., and A. N. DAVISON. 1972. Cholesterol metabolism in myelin and other subcellular fractions of rat brain. *J. Lipid Res.* **13**:563–570.
41. SPRINGER, M. 1974. A simple holder for efficient mass staining of thin sections for electron microscopy. *Stain Technol.* **49**:43–46.
42. STUMPF, W. E. 1968. Subcellular distribution of ^{3}H-estradiol in rat uterus by quantitative autoradiography—a comparison between ^{3}H-estradiol and ^{3}H-norethynodrel. *Endocrinology.* **83**:777–782.
43. TORVIK, A., and R. L. SIDMAN. 1965. Autoradiographic studies on lipid synthesis in the mouse brain during postnatal development. *J. Neurochem.* **12**:555–565.
44. UZMAN, B. G., and E. T. HEDLEY-WHYTE. 1968. Myelin: dynamic or stable? *J. Gen. Physiol.* **51**:(5, Pt.2):8 s-18 s.
45. WILLIAMSON, J. R., and H. VAN DER BOSCH. 1971. High resolution autoradiography with stripping film. *J. Histochem. Cytochem.* **19**:304–309.
46. WOOD, J. G. 1973. The effects of glutaraldehyde and osmium on the proteins and lipids of myelin and mitochondria. *Biochim. Biophys. Acta.* **329**:118–127.